nature water

Article

https://doi.org/10.1038/s44221-023-00139-9

Hybrid photothermal–photocatalyst sheets for solar-driven overall water splitting coupled to water purification

Received: 17 January 2023

Accepted: 30 August 2023

Published online: 13 November 2023

Check for updates

Chanon Pornrungroj[1,2,4], Ariffin Bin Mohamad Annuar[1,4], Qian Wang[1,3], Motiar Rahaman[1], Subhajit Bhattacharjee[1], Virgil Andrei[1] & Erwin Reisner[1]

Photocatalytic water splitting converts sunlight directly into storable hydrogen, but commonly involves the use of pure water and land for plant installation while generating unusable waste heat. Here we report a hybrid device consisting of a photocatalyst (PC) and a solar vapour generator (SVG) for simultaneous overall water splitting and water purification from open water sources. Specifically, an ultraviolet light-absorbing $RhCrO_x$–Al:$SrTiO_3$ PC is deposited on top of a floating, visible and infrared light-absorbing porous carbon SVG, which produces green fuel with a solar-to-hydrogen efficiency of 0.13 ± 0.03% and 0.95 kg m^{-2} h^{-1} of water vapour as the feed for the PC and collectable purified water. This integrated system maintains operational stability in seawater and other aqueous waste streams for over 154 h due to the isolation of the PC from contaminants in the liquid feedstock. This work provides a new concept for developing an off-grid energy production/storage solution and is a first step towards alleviating both energy and water supply challenges.

Photocatalysis can enable solar energy to be stored directly in the form of chemical fuels such as green hydrogen produced from water splitting, but its need for pure water limits its commercial viability, particularly in regions facing water scarcity. Even small amounts of contaminants in the feedstock can severely reduce the lifetime and performance of photocatalytic systems[1], and feasibility analyses often underestimate the cost of purified water and its transportation, which can be as high as US$45 per tonne in some regions[2,3]. Additionally, the use of pure water for hydrogen production may further strain the water supply chain. The frequency and severity of droughts worldwide is expected to increase due to anthropogenic climate change[4,5], and a drought was even declared in the majority of areas in England by the Environment Agency in 2022[6]. The land available for industrial development is also becoming increasingly limited due to competing use for agricultural, commercial and residential purposes[7]. Rising global populations, competing land use and increasing concerns over water and land scarcity justify an urgent need to consider a shift towards alternative water sources for fuel production[8].

The use of untreated water sources such as seawater to drive photocatalytic reactions is increasingly being reported[9–12], but the performance and long-term stability of these systems are low and re-engineering of the co-catalysts is often required for the systems to work under such conditions[11–13], leaving their practicality questionable. Alternatively, using water vapour from untreated water may help to avoid issues such as photocatalyst poisoning and the scattering, reflection and absorption of sunlight by contaminants in the water[14].

Vapour-phase photocatalytic or electrolysis processes have a lower energy requirement for splitting water due to the lower standard Gibbs free energy of formation of gaseous water compared with liquid water ($\Delta G^{\circ}_{H_2O(g)}$ = −228.6 kJ mol^{-1} versus $\Delta G^{\circ}_{H_2O(l)}$ = −237.2 kJ mol^{-1})[15].

[1]Yusuf Hamied Department of Chemistry, University of Cambridge, Cambridge, UK. [2]Department of Chemical Engineering, Faculty of Engineering, Chulalongkorn University, Bangkok, Thailand. [3]Graduate School of Engineering, Nagoya University, Nagoya, Japan. [4]These authors contributed equally: Chanon Pornrungroj, Ariffin Bin Mohamad Annuar. e-mail: reisner@ch.cam.ac.uk

https://doi.org/10.1038/s44221-023-00139-9

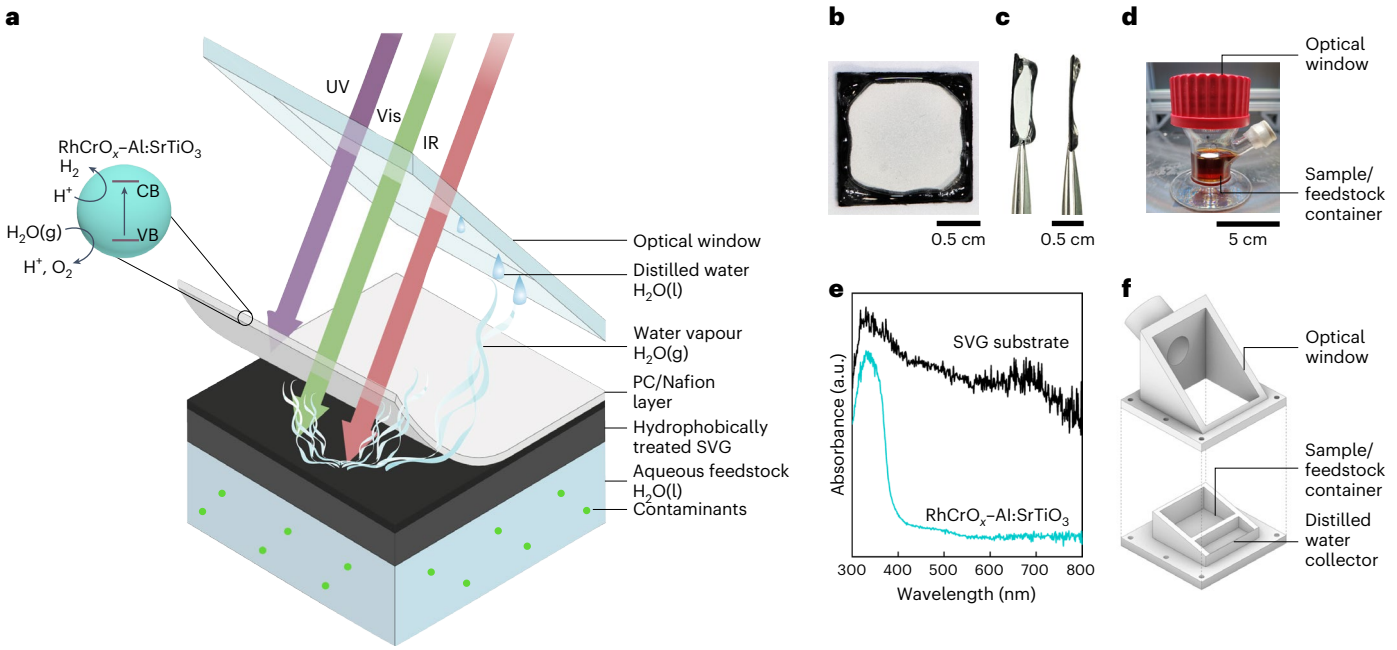

Fig. 1 | Architecture of the hybrid SVG-PC sheets for solar water splitting and purification. a, Illustration of device construction and working principles of the SVG-PC sheet. UV, ultraviolet; Vis, visible; IR, infrared; VB, valence band; CB, conduction band. **b**,**c**, Photographs showing the top (**b**) and side (**c**) views of a SVG-PC sheet held by tweezers (photoactive area of 1 × 1 cm^2). **d**, Experimental set-up for H_2 production consisting of the SVG-PC sheet floating on a turbid feedstock in a top-down photoreactor under AM1.5G illumination. **e**, UV–visible diffuse reflectance spectra of the RhCrO$_x$–Al:SrTiO$_3$ PC and SVG substrate. **f**, Schematic diagram of the photoreactor used to demonstrate integrated water splitting and clean water production. The reactor dimension is 57 × 57 × 47 mm^3 (width × depth × height).

Furthermore, vapour-phase reactions decrease mass transfer resistance and promote the rapid desorption of evolved hydrogen (H_2) and oxygen (O_2) gases, which inhibits back reactions and reduces light scattering[16,17]. However, vapour-phase water splitting systems require complex microreactors for proper gas distribution[18]. This, coupled with the energy-intensive production of water vapour, largely negates the potential advantage of vapour-phase water splitting[18].

Sunlight could be an alternative green energy source to generate water vapour via photothermal conversion devices such as solar vapour generators (SVGs), which can convert most of the solar spectrum into thermal energy to heat water at the liquid–vapour interface. Such devices offer a cost-effective alternative to other water desalination and purification technologies[19]. Carbon-based materials are often used as solar absorbers due to their low cost, ease of fabrication and broad-spectrum solar absorption[20]. Conversely, most photocatalytic water splitting systems can use only high-energy photons to drive the reaction, leaving a large portion of the solar spectrum, particularly the long-wavelength visible and infrared regions, unused[21]. Hence, combining these two solar conversion technologies could provide a light management strategy for the full use of the solar spectrum.

In this study, we addressed the above-mentioned challenges and limitations in current solar fuel systems by integrating two complementary solar technologies, namely a photocatalytic device for the green production of hydrogen from water vapour and an SVG for clean water production. We developed a hybrid photothermal-photocatalyst sheet (Fig. 1a–c) that integrates a photocatalyst (PC) powder on top of an SVG to give a single floating device (SVG-PC). The resulting floating sheet uses the entire solar spectrum due to the synergistic absorption of UV light by the PC top layer and visible–infrared light by the SVG (Fig. 1a,e). Evaporation of the aqueous feedstock by the SVG supplies the PC layer with ample water vapour to generate H_2 and O_2 without the use of sacrificial reagents. The remaining clean water vapour is condensed and collected. The concept of photothermal–photocatalysis has previously been explored in the context of solar vapour generation coupled with the photocatalytic degradation of organic contaminants[13,22–24], but there are only a few examples of overall water splitting[25]. Previous studies employed a design where the PC (solid) interacts with water (liquid) to produce H_2 and O_2 (gas), leading to stability issues, especially when seawater was used[13]. By contrast, our approach offers new insights by using a unique design where the PC (solid) interacts only with water vapour, H_2 and O_2 (gas). This complete separation of the PC from the solution underneath improves the stability and inertness of the physically separated PC towards various dissolved substrates. The versatility of this design could allow off-grid green energy and clean water production in regions facing water and land scarcity.

Assembly of the SVG-PC sheet

Aluminium-doped strontium titanate (Al:SrTiO$_3$) was selected as the UV-active PC material due to its high activity towards overall water splitting, simple synthesis and low cost. The Al:SrTiO$_3$ powder was synthesized following a previously reported flux method (see Methods section)[26,27]. The absorption edge of Al:SrTiO$_3$ of ~380 nm corresponds to a bandgap energy[26] of 3.2 eV (Fig. 1e). Fig. 2a shows a scanning electron microscopy (SEM) image of Al:SrTiO$_3$. The crystal structure of Al:SrTiO$_3$ was confirmed by its powder X-ray diffraction pattern (PXRD; Supplementary Fig. 1). The RhCrO$_x$ hydrogen evolution co-catalyst was loaded onto Al:SrTiO$_3$ (RhCrO$_x$–Al:SrTiO$_3$) by impregnation[28]. The Cr component prevents the water-forming backward reaction of O_2 and H_2 by blocking O_2 from reaching the embedded Rh species[29]. Transmission electron microscopy energy-dispersive X-ray elemental mapping (TEM–EDX) and inductively coupled plasma optical emission spectrometry (ICP-OES) analysis confirmed the conformal deposition of RhCrO$_x$ on Al:SrTiO$_3$ (Fig. 2b, Supplementary Fig. 2 and Supplementary Table 1).

A carbon-based gas diffusion layer comprising a fibrous macroporous bottom layer and a smooth macroporous top layer was selected as the SVG (Fig. 2c and Supplementary Fig. 3). The material provides broadband light absorption, and its porous structure gives it the ability to float on water (density ≈ 0.49 g cm^{-3}) and allows for efficient water

https://doi.org/10.1038/s44221-023-00139-9

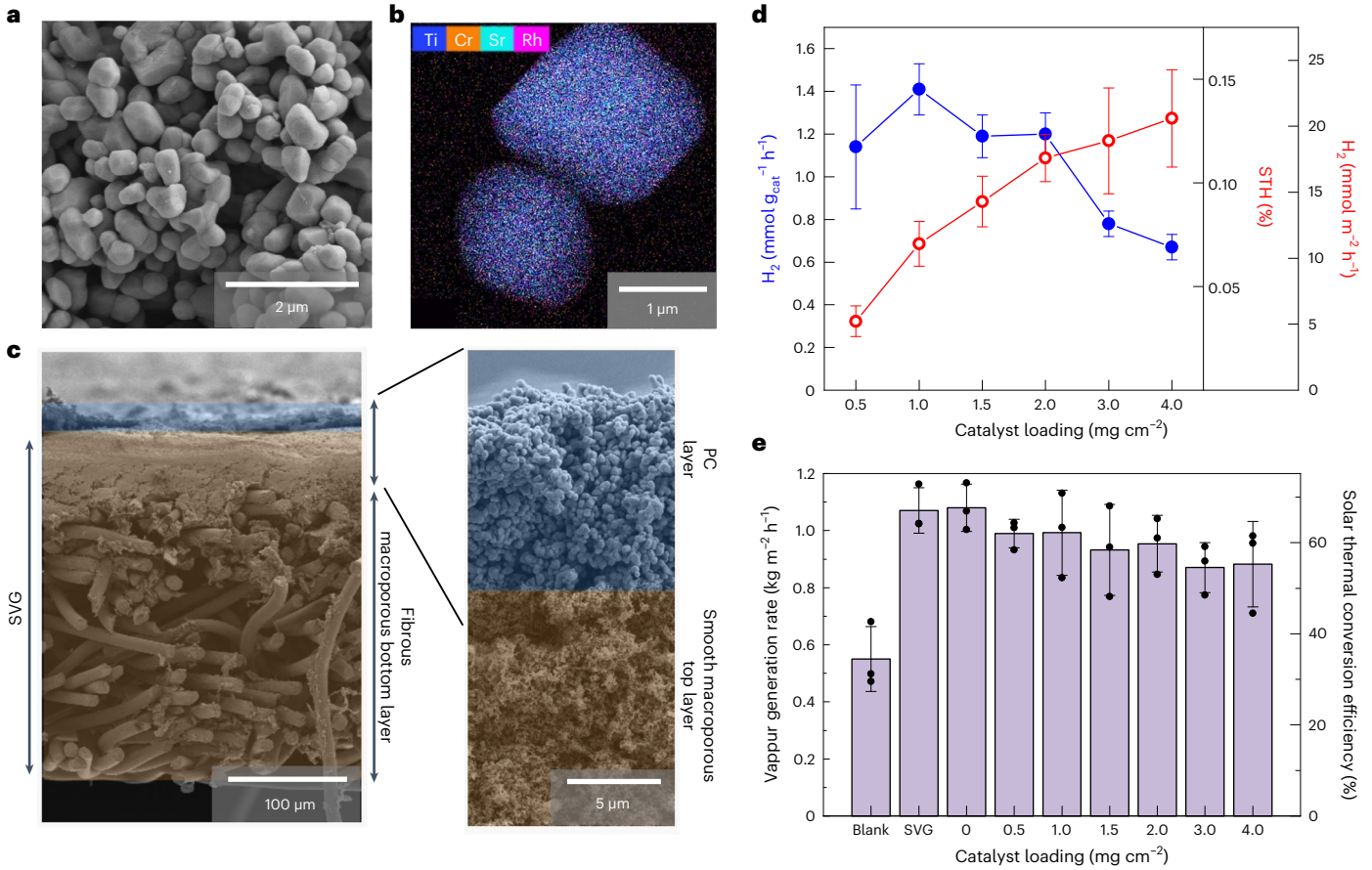

Fig. 2 | Physical characterization and PC loading optimization. a, SEM image of pristine Al:$SrTiO_3$, **b**, TEM–EDX image of the as-prepared $RhCrO_x$–Al:$SrTiO_3$. **c**, Cross-section SEM images of the as-prepared SVG-PC sheet. **d**, Optimization of PC loading for H_2 evolution (The units mmol g_{cat}^{-1} h^{-1} represent mmol per gram catalyst per hour.) Data in red corresponds to both H_2 and STH. **e**, Solar vapour generation rate and solar thermal conversion efficiency for the SVG substrate and SVG-PC sheets. Photocatalytic and solar vapour generation measurements were performed using pure water under AM1.5G illumination for 22 and 4 h, respectively. The data in **d** and **e** are presented as mean values ± SD for reactions performed in triplicate ($n = 3$).

transport (see Supplementary Discussion 1). Additionally, the bilayer construction and macroscopic porous structure of the SVG provide a natural salt rejection pathway preventing salt fouling issues[30]. The floating SVG-PC sheet was fabricated by drop casting $RhCrO_x$–Al:$SrTiO_3$ powder dispersed in isopropanol onto a hydrophobically treated (silanization) SVG substrate, followed by drop casting Nafion solution (Supplementary Fig. 4). Afterward, the sheets were dried at 338 K overnight to ensure removal of isopropanol. The Nafion ionomer was used to better adhere the PC to the SVG and improve the interaction between the PC and the water vapour generated by the SVG, thus increasing the robustness and efficiency of our devices[31–33]. The weight and density of the as-prepared sheets (consisting of SVG, PC powder and optical adhesive) were approximately 37.4 ± 0.1 mg cm^{-2} and 0.67 ± 0.01 g cm^{-3}, respectively, allowing them to intrinsically float on the surface of water without additional support[8]. EDX elemental mapping confirmed the presence of $RhCrO_x$–Al:$SrTiO_3$ on the SVG substrate (Supplementary Fig. 5). The sheets were studied in a top-down reactor under AM1.5G (100 mW cm^{-2}) irradiation for 22 h (Fig. 1d) with H_2 and O_2 quantification by gas chromatography (GC) and a fluorescence oxygen sensor probe, respectively. Subsequently, the vapour generation rates were measured in a 1.5 × 1.5 × 5.0 cm^3 open-top custom-designed reactor (see Methods section).

The optimum PC powder loading of the SVG-PC sheets for both water splitting and water purification was found to be 2.0 mg cm^{-2} (Fig. 2d,e and Supplementary Discussion 2). With this loading, the obtained vapour generation rate of 0.95 ± 0.10 kg m^{-2} h^{-1} (equating to ~53 mol vapour per m^2 per h) agrees well with reported literature values for carbonaceous SVGs (Fig. 2e and Supplementary Tables 2 and 3). The rate of vapour production via the SVG is in excess of that theoretically required to sustain the overall water splitting reaction carried out by $RhCrO_x$–Al:$SrTiO_3$, which requires three orders of magnitude less water than the current SVG output, with the excess water vapour producing distilled water[26].

Seawater splitting and desalination

On average, natural seawater contains 3.1–3.8% salinity and has a pH of 7.5–8.4. It contains various ions, such as Na^+, K^+, Mg^{2+}, Ca^{2+} and Cl^-, with NaCl being the predominant component. Thus far, seawater has rarely been used for solar fuel synthesis using photovoltaic-electrolyser, photoelectrochemical or photocatalytic devices due to their reduced performance as a result of catalyst poisoning and possible side reactions[10,12] (Supplementary Table 4). For liquid-phase seawater splitting using a powder suspension of $RhCrO_x$–Al:$SrTiO_3$ or $RhCrO_x$–Al:$SrTiO_3$ immobilized on a glass substrate (Glass-PC), the H_2 evolution rate decreased more than fourfold and a substantial decrease in the O_2 evolution rate was observed compared with pure water splitting (Fig. 3a, Supplementary Fig. 6 and Supplementary Table 5). This suggests that the performance of $RhCrO_x$–Al:$SrTiO_3$ is strongly inhibited when the particles are in direct contact with seawater. The reduced H_2 evolution may be attributed to the poisoning of a fraction of the H_2 evolution catalyst on direct contact with impurities present in seawater[10,12]. The observed non-stoichiometric H_2/O_2 ratio implies that other oxidation reactions also occur. For example, the oxidation of Cl^- (Cl^-/Cl_2, 1.36 V versus the normal hydrogen electrode at pH 0) in

https://doi.org/10.1038/s44221-023-00139-9

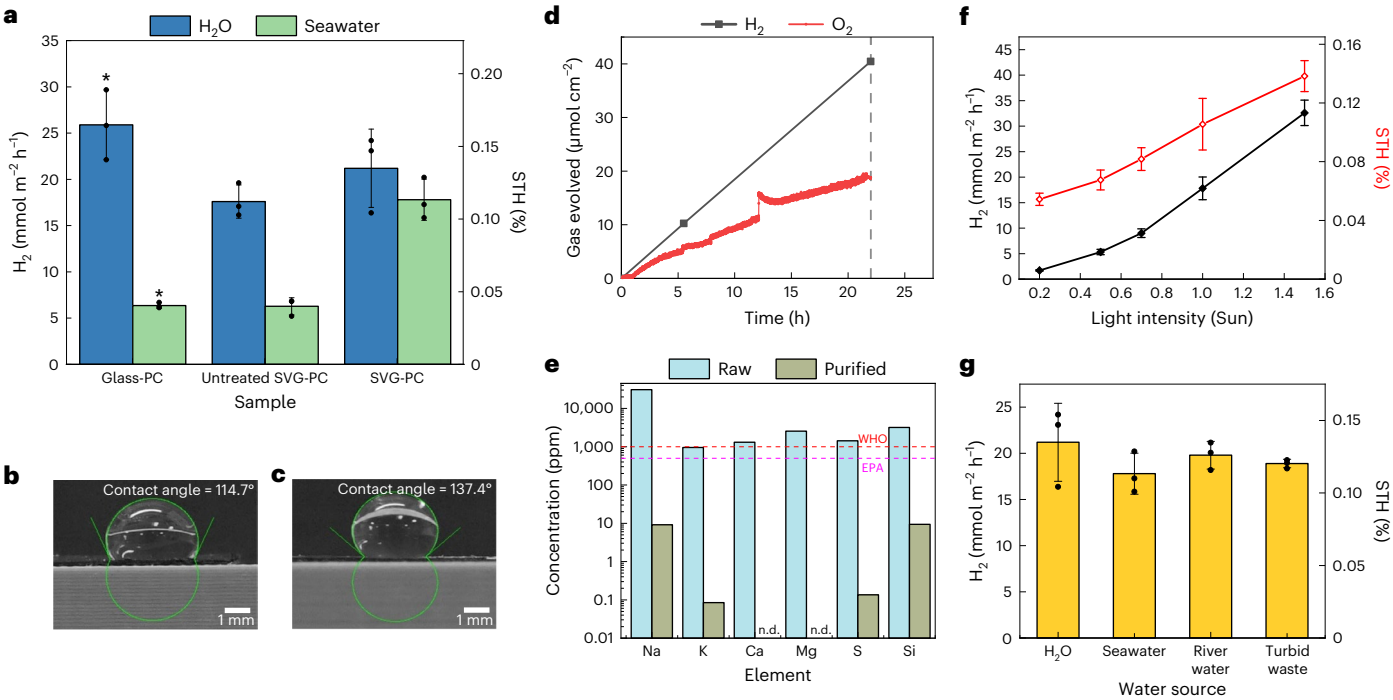

Fig. 3 | SVG-PC sheet for seawater splitting and desalination. a, Photocatalytic performance of $RhCrO_x$–Al:$SrTiO_3$ deposited on glass, SVG or hydrophobically treated SVG in pure water and seawater. The asterisks indicate liquid-phase water splitting. **b**,**c**, Contact angle measurement of a water droplet on pristine SVG (**b**) and hydrophobically treated SVG (**c**). **d**, Time course of H_2 and O_2 evolution via the water splitting reaction using the SVG-PC sheet over artificial seawater. The fluctuations in the O_2 measurements are likely due to the formation of water droplets on the oxygen sensor probe via condensation. The dashed vertical line indicates the time at which the irradiation was ended. **e**, Element content of raw and purified artificial seawater. n.d., not detected. The red and purple dashed horizontal lines indicate the maximum allowable salinity content of drinking water based on standards set by the WHO and EPA, respectively. **f**, H_2 evolution and STH using the SVG-PC sheet under various light intensities. **g**, H_2 evolution and STH from various contaminated water feedstocks using the SVG-PC sheet. The photocatalytic and solar vapour generation measurements were performed under AM1.5G for 22 h at room temperature. The data in **a**, **f** and **g** are presented as mean values ± SD for reactions performed in triplicate ($n = 3$).

seawater might be more favourable because its two-electron oxidation is kinetically easier than the four-electron oxidation of water[34].

Although there already exists a physical separation between the PC layer and aqueous feedstock via the SVG (Fig. 1a), the SVG substrate was also hydrophobically treated before PC deposition to further repel any contaminants dissolved in the bulk solution that might permeate through the SVG top layer to the PC layer. Thus, before PC deposition, the SVG was treated with a silanization solution (2.5 vol% dichlorodimethylsilane (DCDMS) in hexane) to increase its hydrophobicity (Supplementary Fig. 4). The resulting hydrophobically treated SVGs displayed a higher contact angle than untreated samples (Fig. 3b,c and Supplementary Fig. 7), and also showed better water repellency against water droplets than untreated samples (Supplementary Video 1). As a result, our SVG-PC sheet in artificial seawater achieved a H_2 evolution rate and solar-to-hydrogen (STH) efficiency of 17.8 ± 2.2 mmol m^{-2} h^{-1} and 0.11 ± 0.02%, respectively. The values obtained with the SVG-PC were around three times higher than those obtained with the Glass-PC for liquid-phase seawater splitting (Fig. 3a). In contrast to the Glass-PC, near-stoichiometric H_2 and O_2 evolution was achieved from seawater with the SVG-PC (Fig. 3d and Supplementary Table 5). The H_2 evolution rates of the SVG-PC sheet over pure water and seawater were also linear throughout the photocatalytic tests (Supplementary Fig. 8 and Supplementary Table 6). SVG-PC sheets irradiated with only visible–infrared light yielded no H_2, and their performance was halved without the photothermal effect of the SVG (UV irradiation only; Supplementary Fig. 9 and Supplementary Table 7); under UV irradiation alone, the sheets maintained a reasonable performance as the rate of vapour generation was still enhanced by the SVG (Supplementary Fig. 10 and Supplementary Table 8). Further control experiments under full-spectrum irradiation showed that when the SVG-PC sheet was suspended over seawater, without the direct interaction between the SVG and the liquid phase, the H_2 evolution of SVG-PC decreased by an order of magnitude (Supplementary Fig. 11 and Supplementary Table 9). This indicates that localized heating at the liquid–vapour interface by the SVG is crucial for the optimal function of the SVG-PC sheet by maintaining a high flux of water vapour over the PC. The photothermal effect of the SVG was visualized using infrared thermal imaging, which showed a higher local temperature on the SVG compared to the bulk liquid (Supplementary Figs. 12 and 13 and Supplementary Video 2). These results confirm the synergistic effect of the hybrid SVG-PC design for use of the full solar spectrum.

The importance of the hydrophobic treatment in our system was evident when we compared the SVG-PC with a sheet consisting of the PC deposited on a bare SVG (denoted untreated SVG-PC), as shown in Fig. 3a. The seawater splitting rate obtained with the SVG-PC was ~2.8 times greater than that of the untreated SVG-PC. These results imply that without the hydrophobic treatment, some harmful inorganic ions, such as Cl^- and Mg^{2+}, may still be able to reach the PC, allowing side reactions, leading to a lower photocatalytic rate compared with the use of pure water as a feedstock[35] (Supplementary Tables 5 and 10). Note that an overly silanized SVG (>2.5 vol%) may inhibit water evaporation by the SVG and have an adverse effect on the H_2 evolution rate (Supplementary Fig. 14). ICP-OES analysis of the condensed desalinated seawater, collected from the reactor wall after each experiment, showed that the concentrations of Na, K, S and Si were 9.11, 0.09, 0.14 and 9.41 mg l^{-1}, respectively, while the concentrations of Ca and Mg were below the detectable threshold (Fig. 3e, Supplementary Table 11). These numbers are well below the salinity standards of drinking water set by the World

https://doi.org/10.1038/s44221-023-00139-9

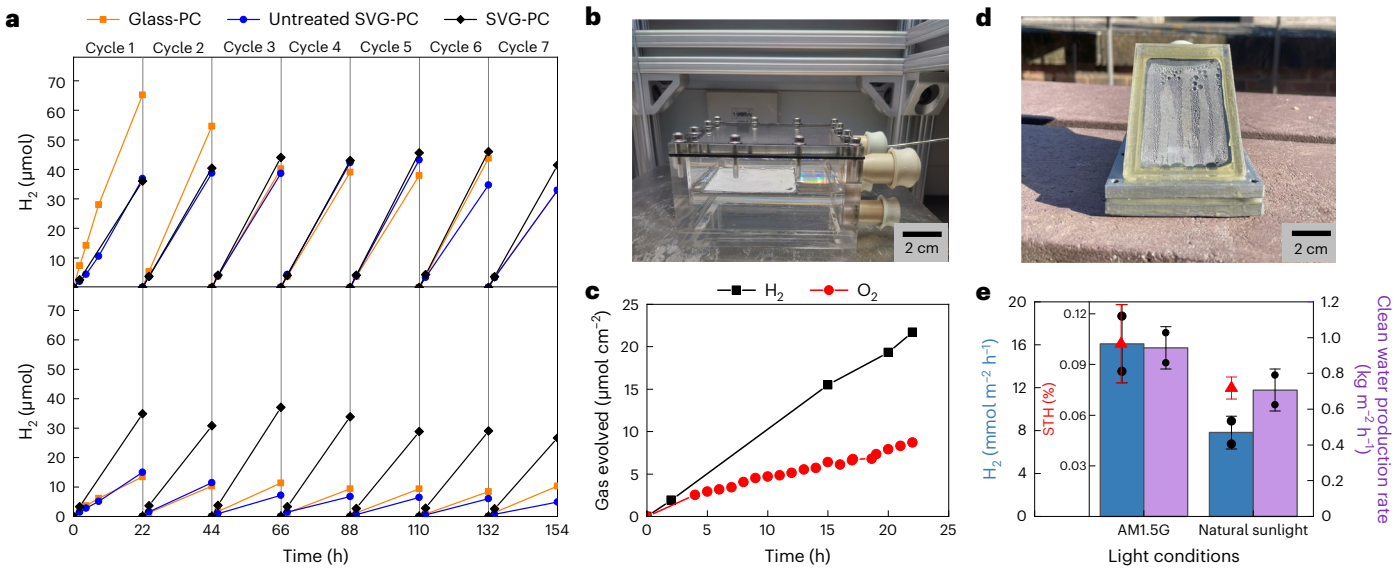

Fig. 4 | Long-term stability, large-scale and integrated SVG-PC set-up. **a**, Long-term H_2 evolution from pure water (top) and seawater (bottom) using Glass-PC, untreated SVG-PC and SVG-PC PC sheets. Photocatalytic measurements were performed under AM1.5G irradiation for 22 h each cycle. The reactor was purged with N_2/CH_4 for 15 min before each cycle. **b**, Photograph of the assembled reactor containing a 25 cm^2 SVG-PC sheet and artificial seawater. **c**, Time course of H_2 and O_2 evolution via the water splitting reaction using a 25 cm^2 SVG-PC sheet over artificial seawater (22 h). **d**, Outdoor set-up for integrated H_2 evolution and clean water production using the SVG-PC sheet with river water. **e**, Integrated H_2 evolution and clean water production rate under simulated and natural sunlight. The photocatalytic experiments were performed under AM1.5G irradiation and natural sunlight for 4 and 2 h, respectively. The data are presented as mean values ± SD for experiments performed in duplicate ($n = 2$).

Health Organization (WHO) and the US Environmental Protection Agency (EPA)[36,37]. Our design yields one of the highest activities among photocatalytic seawater splitting systems while also providing purified water as a secondary product (Supplementary Table 4).

The performance of our devices was then evaluated under 0.2–1.5 Sun irradiation using seawater. The H_2 evolution rate and STH efficiency increased from 1.71 ± 0.1 mmol m^{-2} h^{-1} and 0.06 ± 0.01%, respectively, at 0.2 Sun to 32.6 ± 2.49 mmol m^{-2} h^{-1} and 0.14 ± 0.01%, respectively, at 1.5 Sun (Fig. 3f and Supplementary Table 12). The disproportionate increase in the water splitting rate with increasing light intensity contradicts conventional PC suspension systems, where the rate of water splitting by the PC commonly increases linearly for a light intensity below 1 Sun (ref. 38). It has been reported that the performance of gas-phase water splitting is proportional to the partial pressure of water, which affects the coverage of water molecules on the surface of the PC[18]. Hence, the disproportionate increase in the water splitting rate could be attributed to the fact that the SVG performs more efficiently at a higher light intensity and therefore yields a higher water partial pressure in the reactor for the PC layer[39]. This result suggests that this system could benefit from higher light intensity[40].

Universality and stability of SVG-PC sheets

Next, we evaluated our SVG-PC design using other real-word feedstocks, that is, river water (River Cam, United Kingdom) and turbid industrial waste from the paper industry (Sustainable Fiber Technologies). For the river water, the H_2 evolution rate and STH efficiency were 19.8 ± 1.5 mmol m^{-2} h^{-1} and 0.13 ± 0.01%, respectively (Fig. 3g). These results show that organic material and other contaminants present in river water do not affect the performance of our device. Furthermore, for the turbid waste, the H_2 evolution rate and STH efficiency were 18.9 ± 0.5 mmol m^{-2} h^{-1} and 0.12 ± 0.01%, respectively, demonstrating that light absorption and scattering by the liquid feedstock are avoided entirely because light does not need to travel through the liquid phase to reach the PC. O_2 analysis showed that the H_2 and O_2 evolution ratio of the SVG-PC in the river water and turbid waste were 2.51 and 2.31, respectively (Supplementary Table 5). ICP-OES analysis of the condensed water from each feedstock showed that clean water (meeting WHO and EPA salinity standards for drinking water) was produced in all cases (Supplementary Table 11). Hence, the SVG-PC sheet performs similarly well regardless of the type of water used. These results further validate the versatility of this approach.

For the long-term stability study, we evaluated three different systems (Glass-PC, untreated SVG-PC and SVG-PC) in both pure water and seawater (Fig. 4a). In pure water, Glass-PC initially exhibited a higher photocatalytic performance than the untreated SVG-PC and SVG-PC (Supplementary Discussion 3). These three systems showed STH efficiencies in the first 22 h of 0.17, 0.11 and 0.13%, respectively. However, the activity of the Glass-PC rapidly decreased by over 40% after 66 h. This decrease was attributed to the loss of Cr species from the $RhCrO_x$–Al:$SrTiO_3$ surfaces, as evidenced by a notable decrease in the Cr/Rh ratio from 1.1 to 0.6 after 154 h of irradiation (Supplementary Table 1). Conversely, both the untreated SVG-PC and SVG-PC were stable up to 154 h in pure water, with the former retaining 89% of its initial performance and the latter seeing no noticeable change in performance. The performance of the SVG-PC sheet had already surpassed the performance of the Glass-PC by the end of the third cycle (≥66 h). In artificial seawater, the performance of the Glass-PC and the untreated SVG-PC was considerably lower than their performance in pure water. Both systems showed an STH efficiency of only 0.04% in the first 22 h, and their H_2 evolution rates continued to decrease in later cycles. Conversely, the SVG-PC performed similarly in both seawater and pure water. Even in artificial seawater, the system retained 80% of its initial performance after 154 h (Supplementary Table 13). The slight decrease in performance in seawater may be due to a small amount of PC being exposed to the liquid phase. Contact angle measurements showed that the SVG-PC retained its hydrophobicity to a far greater extent than the untreated SVG-PC after 154 h of operation (Supplementary Fig. 15). Thus, the hydrophobically treated SVG not only separates the PC from contaminants in seawater, but also prevents co-catalyst dissolution by keeping the PC relatively dry. This was verified by ICP-OES analysis of the SVG-PC after catalysis, which showed that the

Rh and Cr content of the SVG-PC remained constant (Supplementary Table 1). SEM images also showed no apparent difference between the as-prepared and used SVG-PC sheets (Supplementary Figs. 5 and 16). Furthermore, there was no noticeable salt accumulation on the SVG substrate for the sample tested in seawater.

The scalability of our system was demonstrated by using a 25 cm^2 SVG-PC sheet (Fig. 4b). The weight (19.8 ± 0.1 mg cm^{-2}) and density (0.44 ± 0.02 g cm^{-3}) of the sheets were reduced in the large-scale samples compared with their 1 cm^2 counterparts. In artificial seawater, the H_2 evolution rate and STH efficiency of the large sheet were 9.87 mmol m^{-2} h^{-1} and 0.063%, respectively. The drop in performance can be attributed to a decrease in incident light due to water condensation and the use of Plexiglass as the reactor window, as well as to gas leakage that might occur in the scaled-up reactor. However, stoichiometric overall water splitting (H_2/O_2 ratio of 2.4) was again achieved (Fig. 4c and Supplementary Fig. 17). Thus, the potential scalability of the hybrid device was successfully demonstrated.

Finally, we used a custom-designed photoreactor (Fig. 1f) to demonstrate integrated water splitting and clean water production using water from the River Cam. In the reactor, H_2 from water splitting was trapped in the gas-tight headspace of the reactor while condensed water vapour from the SVG formed droplets on the sloped window, which flowed down into a separate partition for collection (Fig. 4d and Supplementary Figs. 18 and 19). Figure 4e shows that under AM1.5G irradiation, the H_2 evolution and clean water production rate of the SVG-PC were 16.1 ± 3.6 mmol m^{-2} h^{-1} (STH: 0.10 ± 0.02%) and 0.94 ± 0.12 kg m^{-2} h^{-1}, respectively (Supplementary Table 14). These values are similar to those obtained from separate H_2 evolution and water evaporation experiments, thus confirming the successful demonstration of simultaneous water splitting and clean water production by the SVG-PC sheet. The slight drop in performance can be attributed to the scattering of light from the water layer and droplets formed on the tilted window of the integrated reactor. This could be avoided by hydrophobically treating the reactor window via silanization to improve the formation and flow of water down the window[41]. Under natural sunlight, a consistent STH of 0.08 ± 0.01% was achieved, while the H_2 evolution and clean water production rate dropped to 7.82 ± 1.52 mmol m^{-2} h^{-1} and 0.71 ± 0.12 kg m^{-2} h^{-1}, respectively. The decline in the overall products in the outdoor experiments is likely due to the lower incident light intensity over the course of the outdoor experiments (average of ~0.6 Sun; Supplementary Fig. 20a,b). Our techno-economic analysis reveals that the proposed hybrid SVG-PC sheets have potential economic advantages over existing PC panels where the cost of water purification and land use are more expensive in a real-world scenario (Supplementary Table 15 and Supplementary Discussion 4).

Overall, these findings provide the proof of concept of a full-spectrum-powered SVG-PC device for the production of solar fuel and clean water from polluted open water sources. By integrating the complementary UV absorption of a PC with a broadband light-absorbing SVG, the full solar spectrum can be used with minimal compromise on hydrogen and water production compared with their non-integrated counterparts. Without requiring direct contact between the PC and the aqueous liquid phase, the photocatalytic process can take place directly on top of a variety of aqueous feedstocks without having to modify the PC. H_2 production from contaminated feedstocks via conventional photocatalytic, photoelectrochemical and photovoltaic-electrolysis systems suffers from catalyst poisoning. The SVG-PC device designed in this study circumvents this issue, and its potential use on a range of open-water sources, whether it be a river, sea, water reservoir or industrial waste, also suggests great potential for reducing competition for land and lowering the cost of water purification in energy production as well as providing clean water[8].

This approach could be extended to a range of other photocatalytic and photothermal materials[42]. Although the performance of the current system is limited by the light absorption of the model PCs, the activity may be improved further through the use of different photocatalytic materials[42], a Z scheme assembly[43], solar concentration and more efficient SVGs for water evaporation[20]. While the reaction temperature when using liquid water is limited to less than 100 °C, which limits the use of highly concentrated solar irradiation (without external cooling), this design opens up the possibility of using concentrated solar light to enhance photocatalytic activity and improve scalability. This design approach could be used in a large-scale floating plant and can benefit from the use of parabolic solar concentrators to enhance photocatalytic activity and solar fuel production efficiency as well as to reduce the amount of active material to save costs, as we propose in Supplementary Fig. 21. A membrane gas separation unit could also be incorporated into the hypothetical floating plant to prevent pressure build-up and ensure that the hydrogen and oxygen gas mixture remains outside explosive limits[44]. The concept explored in this study has also the potential to be adapted to other moisture-harvesting systems, such as atmospheric water harvesters using a metal–organic framework for similar applications in arid areas[45]. Due to both supply and logistical challenges, over 2 billion people live in regions experiencing high water stress and about 730 million people do not have access to modern electricity infrastructure. The hybrid SVG-PC sheet device introduced in this work offers a potential pathway towards decentralized fuel production, energy storage and clean water production to support the needs of developing regions experiencing energy and water scarcity.

Methods

Materials

$SrTiO_3$ (99.9%, Wako), Al_2O_3 nanopowder (Sigma-Aldrich), $SrCl_2$ (99.99%, Merck), $Na_3RhCl_6{\cdot}nH_2O$ (17.8 wt% Rh, Mitsuwa), $Cr(NO_3)_3{\cdot}9H_2O$ (98.0–103.0%, Kanto), Nafion (~5%, Sigma-Aldrich), isopropanol (≥99.5%, Sigma-Aldrich), DCDMS (~5%, Sigma-Aldrich), heptane (≥99%, Sigma-Aldrich), nitric acid (67–69%, Fisher Scientific), carbon paper (Freudenberg H23C2, Freudenberg Performance Materials), optical adhesive (NOA 63, Norland Products), artificial seawater (liquid, Reagecon), river water (collected from the River Cam, Darwin College, University of Cambridge, UK) and turbid wastewater (collected from Sustainable Fiber Technologies) were used without further purification unless otherwise stated.

Synthesis of Al:$SrTiO_3$

Al:$SrTiO_3$ was prepared using a flux method following a previously reported procedure[27]. $SrTiO_3$, Al_2O_3 nanopowder and $SrCl_2$ were mixed in a molar ratio of 1:0.02:10 using an agate mortar. The mixture was then heated in an alumina crucible at 1,423 K for 10 h and subsequently cooled to room temperature, after which the product was stirred in 500 ml Milli-Q water. The resulting powder was collected by filtration to remove any impurities associated with $SrCl_2$. This rinsing process was repeated three times. The resulting Al:$SrTiO_3$ powder was dried at 338 K in an oven overnight.

Co-catalyst loading

Al:$SrTiO_3$ powder was loaded with $RhCrO_x$ (0.1 wt% Rh and 0.1 wt% Cr) by impregnation from an aqueous solution of Na_3RhCl_6 and $Cr(NO_3)_3$, followed by calcination at 623 K for 1 h in air following a previously reported procedure[27].

PC sheet fabrication

To fabricate the floating PC sheets for vapour-phase water splitting, carbon paper was cut into 1.4 cm × 1.4 cm sheets and a thin layer of optical glue was applied to the perimeter of the sheets. The carbon paper , which functions as the SVG, consists of a smooth macroporous top layer upon which the PC can be deposited, as well as a fibrous macroporous bottom layer which enables the sheets to float and allows for efficient water vapour transport through the sheet. The optical glue mask acts as a second layer of protection to prevent the PC layer from being

exposed to the liquid feedstock. The sheets were then placed in a UV/ozone cleaner for 20 min to cure the glue and remove possible organic material from the surfaces of the sheets. A hydrophobic coating was applied to the sheets following a modified literature procedure[46]. In brief, DCDMS and heptane were mixed in a volume ratio of 2:1 and the sheets were immersed in this solution for 1 h. After rinsing in heptane, the sheets were heat-treated at 423 K for 30 min.

For PC deposition, 2 mg $RhCrO_x$–Al:$SrTiO_3$ was added to 200 µl isopropanol and the mixture ultrasonicated for about 1 min until the catalyst was well dispersed. This catalyst mixture was drop cast onto the carbon paper in four equal layers (50 µl per layer), with the sheets allowed to dry between each successive layer. Next, 2 µl Nafion solution was diluted in 50 µl isopropanol and then drop cast onto the sheets. The sheets were then dried at 338 K overnight (Supplementary Fig. 4).

Submerged PC sheets for liquid-phase water splitting were prepared following a similar procedure but with several key differences. After applying the layer of optical glue onto glass sheets and treatment in a UV/ozone cleaner, $RhCrO_x$–Al:$SrTiO_3$ was deposited onto the glass without the addition of Nafion. The glue mask was then removed and the sheets annealed at 673 K for 1 h.

Material characterization

UV–visible diffuse reflectance spectra were recorded on a Varian Cary 60 Bio spectrophotometer equipped with a Harrick Scientific Video Barrelino probe. A TESCAN MIRA3 field emission gun-scanning electron microscope equipped with an Oxford Instruments Aztec Energy X-maxN 80 EDS system was used for SEM and EDX mapping. PXRD patterns of the samples were measured with a PANalytical Empyrean Series 2 diffractometer using Cu K_α irradiation operated at 40 kV and 40 mA. ICP-OES was performed on a Thermo Scientific iCAP 700 spectrometer at the University of Cambridge Microanalysis Service (Department of Chemistry).

Photocatalytic reaction

All the photocatalytic measurements were conducted in custom-designed top-irradiation-type glass photoreactors with a screw-top cap and a quartz window (Supplementary Fig. 22). First, 10 ml H_2O or other water source was added to the photoreactor. The liquid was purged with N_2 (containing 2% CH_4 as an internal standard for gas chromatographic analysis) for 30 min. All purging needle holes were then sealed with Loctite Superglue universal adhesive. The prepared floating PC sheets were then placed on the surface of the liquid (note that the submerged PC sheets were placed directly in the liquid) and the headspace of the photoreactor was purged with the same N_2/CH_4 mixture for 15 min. The sheets were then irradiated using a solar light simulator (G2V Sunbrick LED Solar Simulator) at AM1.5G irradiance; the light irradiation was calibrated in the range of 10–100 mW cm^{-2} using a certified Newport 843-R optical power meter. The experiments were conducted without stirring and temperature control. H_2 evolution was measured at set times (0, 2, 4, 8 and 22 h) by GC. At each sampling time, a 50 µl gas sample was taken from the headspace of the photoreactors and analysed using a Shimadzu GC-2010 Plus gas chromatograph equipped with a barrier discharge ionization detector. To avoid any aerobic leakage, O_2 was quantified separately inside a Belle Technology glove box under an inert atmosphere. The O_2 evolution was monitored using a NeoFox-GT fluorometer and Fospor-R fluorescence oxygen sensor probe (Ocean Optics). The H_2/O_2 ratio was calculated from the gas accumulated after 22 h of experiment. For the long-term experiments, the reactors were purged with the N_2/CH_4 mixture for 15 min before each cycle (no washing or substrate change took place between cycles). For the integrated set-up, 1 × 1 cm^2 SVG-PC sheets were tested in a three-dimensional (3D)-printed reactor (Supplementary Figs. 18 and 19). The reactor was printed using CPE+ (co-polyester) filament with UV-transmitting Plexiglass attached to the top part of the cell using two-part epoxy. The 25 cm^2 SVG-PC sheets were tested in a custom-made, one-compartment reactor (Fig. 4b).

The STH efficiency of this system was calculated using equation (1), where r_{H_2} is the rate of H_2 evolution, ΔG° is the Gibbs free energy of reaction (237 kJ mol^{-1} for liquid-phase and 228.6 kJ mol^{-1} for vapour-phase overall water splitting under standard conditions at 298 K), P_{light} is the energy flux of the incident sunlight and A is the device photoactive area[27] (measured using ImageJ software, as shown in Supplementary Fig. 23).

$$\mathrm{STH}\,(\%) = \frac{\text{Energy output as } H_2}{\text{Incident solar light energy}} = \frac{r_{H_2} \times \Delta G^\circ}{P_{light} \times A} \times 100 \quad (1)$$

Water evaporation rate measurement

Open-top containers with an irradiation area of 1.5 cm × 1.5 cm were designed at SolidWorks and fabricated using an Ultimaker 2 Extended+ 3D printer for the water evaporation experiments[47] (Supplementary Fig. 24). The containers were filled with H_2O and the floating PC sheets were placed on the liquid surface. The samples were irradiated using a solar light simulator (G2V Sunbrick LED Solar Simulator) at AM1.5G irradiance. Note that factors such as temperature, humidity and wind speed could adversely affect the evaporation rate of an open system during testing. To avoid these potential issues, a constant room temperature and humidity level were maintained in the laboratory environment. The water evaporation rate was calculated from the change in the mass of the reservoir. For the integrated set-up, the generated water vapour condensed on the tilted window of the reactor and flowed down into a separate compartment (Supplementary Figs. 18 and 19). After experiments, this water was collected and weighed to quantify the clean water produced by the device. The solar thermal conversion efficiency (η) was also calculated using equation (2)[48]:

$$\eta = \frac{m h_{LV}}{I} \quad (2)$$

where m is the evaporation rate, h_{LV} is the total enthalpy of the liquid–vapour phase change of H_2O (2,256 kJ kg^{-1}) and I is the irradiation intensity.

Purified water characterization

Solar vapour generation using the floating PC sheets over artificial seawater, river water and turbid paper mill wastewater was conducted in the same reactors as used for the photocatalytic reactions. Condensed water vapour inside the reactors was collected and analysed by ICP-OES to determine the content of elements commonly found in these water sources (Na, K, Ca, Mg, S and Si).

Statistics

Average values are based on measurements performed in triplicate, except for the integrated and large-scale experiments, where the values are based on measurements performed in duplicate or as a single experiment, respectively. The errors correspond to the standard deviation of data points from individual samples.

Reporting summary

Further information on research design is available in the Nature Portfolio Reporting Summary linked to this article.

Data availability

The data supporting the findings of this study are available within the paper and its Supplementary Information.

References

1. Dingenen, F. & Verbruggen, S. W. Tapping hydrogen fuel from the ocean: a review on photocatalytic, photoelectrochemical and electrolytic splitting of seawater. *Renew. Sustain. Energy Rev.* **142**, 110866 (2021).

2. *Water: At What Cost? The State of the World's Water* (WaterAid, 2016).
3. Sathre, R. et al. Life-cycle net energy assessment of large-scale hydrogen production via photoelectrochemical water splitting. *Energy Environ. Sci.* **7**, 3264–3278 (2014).
4. IPCC *Climate Change 2022: Impacts, Adaptation and Vulnerability* (eds Pörtner, H.-O. et al.) (Cambridge Univ. Press, 2022).
5. Krishnamurthy, R., Fisher, P. K., Choularton, J. B. & Kareiva, P. M. Anticipating drought-related food security changes. *Nat. Sustain.* **5**, 956–964 (2022).
6. *Monthly Water Situation Report: England—August 2022* (Environmental Agency, 2022); www.gov.uk/environment-agency
7. *FAOSTAT: Land Use* (FAO, accessed 22 August 2022); http://www.fao.org/faostat/en/#data/RL
8. Andrei, V. et al. Floating perovskite-$BiVO_4$ devices for scalable solar fuel production. *Nature* **608**, 518–522 (2022).
9. Jin, H. et al. Single-crystal nitrogen-rich two-dimensional Mo_5N_6 nanosheets for efficient and stable seawater splitting. *ACS Nano* **12**, 12761–12769 (2018).
10. Guan, X. et al. Efficient unassisted overall photocatalytic seawater splitting on GaN-based nanowire arrays. *J. Phys. Chem. C* **122**, 13797–13802 (2018).
11. Li, H., Tang, Q., He, B. & Yang, P. Robust electrocatalysts from an alloyed Pt–Ru–M (M = Cr, Fe, Co, Ni, Mo)-decorated Ti mesh for hydrogen evolution by seawater splitting. *J. Mater. Chem. A* **4**, 6513–6520 (2016).
12. Achilleos, D. S., Kasap, H. & Reisner, E. Photocatalytic hydrogen generation coupled to pollutant utilisation using carbon dots produced from biomass. *Green Chem.* **22**, 2831–2839 (2020).
13. Gao, M., Peh, C. K., Zhu, L., Yilmaz, G. & Ho, G. W. Photothermal catalytic gel featuring spectral and thermal management for parallel freshwater and hydrogen production. *Adv. Energy Mater.* **10**, 2000925 (2020).
14. Khan, M. et al. Seawater electrolysis for hydrogen production: a solution looking for a problem? *Energy Environ. Sci.* **14**, 4831–4839 (2021).
15. Spurgeon, J. M. & Lewis, N. S. Proton exchange membrane electrolysis sustained by water vapor. *Energy Environ. Sci.* **4**, 2993–2998 (2011).
16. Verbruggen, S. W. TiO_2 photocatalysis for the degradation of pollutants in gas phase: from morphological design to plasmonic enhancement. *J. Photochem. Photobiol.* **24**, 64–82 (2015).
17. Yoshida, H., Yamada, R. & Yoshida, T. Platinum cocatalyst loaded on calcium titanate photocatalyst for water splitting in a flow of water vapor. *ChemSusChem* **12**, 1958–1965 (2019).
18. Dionigi, F. et al. Gas phase photocatalytic water splitting with $Rh_{2-y}Cr_yO_3$/GaN:ZnO in μ-reactors. *Energy Environ. Sci.* **4**, 2937–2942 (2011).
19. Elimelech, M. & Phillip, W. A. The future of seawater desalination: energy, technology, and the environment. *Science* **333**, 712–717 (2011).
20. Zhao, F., Guo, Y., Zhou, X., Shi, W. & Yu, G. Materials for solar-powered water evaporation. *Nat. Rev. Mater.* **5**, 388–401 (2020).
21. Pornrungroj, C., Andrei, V. & Reisner, E. Thermoelectric-photoelectrochemical water splitting under concentrated solar irradiation. *J. Am. Chem. Soc.* **145**, 13709–13714 (2023).
22. Lu, Y., Zhang, H., Fan, D., Chen, Z. & Yang, X. Coupling solar-driven photothermal effect into photocatalysis for sustainable water treatment. *J. Hazard. Mater.* **423**, 127128 (2022).
23. Han, H., Huang, K., Yao, Y., Li, Z. & Meng, X. Enhanced photocatalytic splitting of photothermally induced water vapor to evolve hydrogen. *Chem. Eng. J.* **450**, 138419 (2022).
24. Lee, W. H. et al. Floatable photocatalytic hydrogel nanocomposites for large-scale solar hydrogen production. *Nat. Nanotechnol.* **18**, 754–762 (2023).
25. Guo, S., Li, X., Li, J. & Wei, B. Boosting photocatalytic hydrogen production from water by photothermally induced biphase systems. *Nat. Commun.* **12**, 1343 (2021).
26. Takata, T. et al. Photocatalytic water splitting with a quantum efficiency of almost unity. *Nature* **581**, 411–414 (2020).
27. Goto, Y. et al. A particulate photocatalyst water-splitting panel for large-scale solar hydrogen generation. *Joule* **2**, 509–520 (2018).
28. Lyu, H. et al. An Al-doped $SrTiO_3$ photocatalyst maintaining sunlight-driven overall water splitting activity for over 1000 h of constant illumination. *Chem. Sci.* **10**, 3196–3201 (2019).
29. Yoshida, M. et al. Role and function of noble-metal/Cr-layer core/shell structure cocatalysts for photocatalytic overall water splitting studied by model electrodes. *J. Phys. Chem. C* **113**, 10151–10157 (2009).
30. Ni, G. et al. A salt-rejecting floating solar still for low-cost desalination. *Energy Environ. Sci.* **11**, 1510–1519 (2018).
31. Gulati, S. et al. Photocatalytic hydrogen evolution on Si photocathodes modified with bis(thiosemicarbazonato)nickel(II)/Nafion. *Chem. Commun.* **55**, 9440–9443 (2019).
32. Li, X. et al. Wettability of Nafion and Nafion/Vulcan carbon composite films. *Langmuir* **28**, 6698–6705 (2012).
33. Uekert, T., Bajada, M. A., Schubert, T., Pichler, C. M. & Reisner, E. Scalable photocatalyst panels for photoreforming of plastic, biomass and mixed waste in flow. *ChemSusChem* **14**, 4190–4197 (2021).
34. Ayyub, M. M., Chhetri, M., Gupta, U., Roy, A. & Rao, C. Photochemical and photoelectrochemical hydrogen generation by splitting seawater. *Chem. Eur. J.* **24**, 18455–18462 (2018).
35. Gao, M., Connor, P. K. N. & Ho, G. W. Plasmonic photothermic directed broadband sunlight harnessing for seawater catalysis and desalination. *Energy Environ. Sci.* **9**, 3151–3160 (2016).
36. *2006 Edition of the Drinking Water Standards and Health Advisories* (US EPA, accessed 1 October 2022); https://agri.idaho.gov/main/wp-content/uploads/2018/03/epa_drinking_water_standard-2006.pdf
37. National Research Council *Review of the Desalination and Water Purification Technology Roadmap* (National Academies Press, 2004).
38. Hisatomi, T., Maeda, K., Takanabe, K., Kubota, J. & Domen, K. Aspects of the water splitting mechanism on $(Ga_{1-x}Zn_x)(N_{1-x}O_x)$ photocatalyst modified with $Rh_{2-y}CryO_3$ cocatalyst. *J. Phys. Chem. C* **113**, 21458–21466 (2009).
39. Zhao, F. et al. Highly efficient solar vapour generation via hierarchically nanostructured gels. *Nat. Nanotechnol.* **13**, 489–495 (2018).
40. Wang, Q., Pornrungroj, C., Linley, S. & Reisner, E. Strategies to improve light utilization in solar fuel synthesis. *Nat. Energy* **7**, 13–24 (2021).
41. Zhai, L. et al. Patterned superhydrophobic surfaces: toward a synthetic mimic of the Namib Desert beetle. *Nano Lett.* **6**, 1213–1217 (2006).
42. Wang, Q. et al. Oxysulfide photocatalyst for visible-light-driven overall water splitting. *Nat. Mater.* **18**, 827–832 (2019).
43. Wang, Q. et al. Particulate photocatalyst sheets based on carbon conductor layer for efficient Z-scheme pure-water splitting at ambient pressure. *J. Am. Chem. Soc.* **139**, 1675–1683 (2017).
44. Nishiyama, H. et al. Photocatalytic solar hydrogen production from water on a 100-m^2 scale. *Nature* **598**, 304–307 (2021).
45. Kim, H. et al. Water harvesting from air with metal-organic frameworks powered by natural sunlight. *Science* **356**, 430–434 (2017).
46. Yang, R. et al. Construction of hydrophobic wood surface and mechanical property of wood cell wall on nanoscale modified by dimethyldichlorosilane. In *IOP Conference Series: Materials Science and Engineering* (IOP Publishing, 2018).
47. Andrei, V. et al. Scalable triple cation mixed halide perovskite–$BiVO_4$ tandems for bias-free water splitting. *Adv. Energy Mater.* **8**, 1801403 (2018).
48. Bae, K. et al. Flexible thin-film black gold membranes with ultrabroadband plasmonic nanofocusing for efficient solar vapour generation. *Nat. Commun.* **6**, 10103 (2015).

Acknowledgements
This work was supported by the Cambridge Trust (Cambridge Thai Foundation Award to C.P. and HRH The Prince of Wales Commonwealth Scholarship to S.B.), the Petronas Education Sponsorship Programme for Postgraduate Studies (to A.B.M.A.), the European Commission for Horizon 2020 Marie Skłodowska-Curie Individual European Fellowships (GAN 793996 to Q.W. and GAN 839763 to M.R.), a Trinity-Henry Barlow Scholarship (to C.P.), the Cambridge Philosophical Society (to C.P.), the JST Fusion Oriented Research for disruptive Science and Technology Program (GAN JPMJFR213D to Q.W.), the Winton Programme for the Physics of Sustainability and St John's College (Title A Research Fellowship to V.A.), and a European Research Council Consolidator (MatEnSAP, GAN 682833 to E.R.) and Proof of Concept Grant (SolReGen to E.R.). We thank H. Greer (University of Cambridge) for assistance with electron microscopy, S. Rodriguez Jimenez for the design of the top-down glass reactor, S. Dey for help with the furnace, C. Pichler for supplying turbid waste substrate, and E. Lam and M. Stanton (University of Cambridge) for useful feedback on the manuscript.

Author contributions
C.P. and E.R. designed the project. C.P., M.R., S.B. and Q.W. developed the device prototypes. C.P. and Q.W. synthesized and conducted the physical characterizations of the semiconductor. C.P. and A.B.M.A. prepared and conducted the physical and photocatalytic characterization of the devices. A.B.M.A. designed and performed solar vapour measurements. A.B.M.A. and M.R. conducted ICP-OES measurements. C.P. developed the integrated reactor with aid on 3D printing from V.A. C.P., A.B.M.A. and V.A. prepared and characterized large-scale samples. C.P. and A.B.M.A. drafted the manuscript with E.R. All authors analysed the data, discussed the results and assisted with manuscript preparation. E.R. supervised the project.

Competing interests
The authors declare no competing interests.

Additional information
Supplementary information The online version contains supplementary material available at https://doi.org/10.1038/s44221-023-00139-9.

Correspondence and requests for materials should be addressed to Erwin Reisner.

Peer review information *Nature Water* thanks Hailiang Wang and the other, anonymous, reviewer(s) for their contribution to the peer review of this work.

nature portfolio

Corresponding author(s): Erwin Reisner

Last updated by author(s): Feb 2, 2023

Reporting Summary

Nature Portfolio wishes to improve the reproducibility of the work that we publish. This form provides structure for consistency and transparency in reporting. For further information on Nature Portfolio policies, see our Editorial Policies and the Editorial Policy Checklist.

Statistics

For all statistical analyses, confirm that the following items are present in the figure legend, table legend, main text, or Methods section.

n/a	Confirmed	
☒	☐	The exact sample size (*n*) for each experimental group/condition, given as a discrete number and unit of measurement
☐	☒	A statement on whether measurements were taken from distinct samples or whether the same sample was measured repeatedly
☒	☐	The statistical test(s) used AND whether they are one- or two-sided *Only common tests should be described solely by name; describe more complex techniques in the Methods section.*
☒	☐	A description of all covariates tested
☒	☐	A description of any assumptions or corrections, such as tests of normality and adjustment for multiple comparisons
☐	☒	A full description of the statistical parameters including central tendency (e.g. means) or other basic estimates (e.g. regression coefficient) AND variation (e.g. standard deviation) or associated estimates of uncertainty (e.g. confidence intervals)
☒	☐	For null hypothesis testing, the test statistic (e.g. *F*, *t*, *r*) with confidence intervals, effect sizes, degrees of freedom and *P* value noted *Give P values as exact values whenever suitable.*
☒	☐	For Bayesian analysis, information on the choice of priors and Markov chain Monte Carlo settings
☒	☐	For hierarchical and complex designs, identification of the appropriate level for tests and full reporting of outcomes
☒	☐	Estimates of effect sizes (e.g. Cohen's *d*, Pearson's *r*), indicating how they were calculated

Our web collection on statistics for biologists contains articles on many of the points above.

Software and code

Policy information about availability of computer code

Data collection	Does not apply
Data analysis	Does not apply

For manuscripts utilizing custom algorithms or software that are central to the research but not yet described in published literature, software must be made available to editors and reviewers. We strongly encourage code deposition in a community repository (e.g. GitHub). See the Nature Portfolio guidelines for submitting code & software for further information.

Data

Policy information about availability of data

All manuscripts must include a data availability statement. This statement should provide the following information, where applicable:

- Accession codes, unique identifiers, or web links for publicly available datasets
- A description of any restrictions on data availability
- For clinical datasets or third party data, please ensure that the statement adheres to our policy

Raw data that support the findings of this manuscript are available from the University of Cambridge data repository (DOI to be added upon acceptance of manuscript)

Human research participants

Policy information about studies involving human research participants and Sex and Gender in Research.

Reporting on sex and gender	Does not apply
Population characteristics	Does not apply
Recruitment	Does not apply
Ethics oversight	Does not apply

Note that full information on the approval of the study protocol must also be provided in the manuscript.

Field-specific reporting

Please select the one below that is the best fit for your research. If you are not sure, read the appropriate sections before making your selection.

☐ Life sciences ☐ Behavioural & social sciences ☒ Ecological, evolutionary & environmental sciences

For a reference copy of the document with all sections, see nature.com/documents/nr-reporting-summary-flat.pdf

Ecological, evolutionary & environmental sciences study design

All studies must disclose on these points even when the disclosure is negative.

Study description	This research describes a new hybrid device for simultaneous water splitting and purification from open water sources. The device combines a photocatalyst (PC) and a solar vapour generator (SVG) to produce storable hydrogen fuel and purified water. Triplicate reporting is done to ensure accuracy and precision in the results, as well as to validate the reproducibility of the experiment. By averaging the three measurements, random errors can be reduced and the overall reliability of the data can be improved. Additionally, it can help detect systematic errors in the experimental setup, data recording, or analysis.
Research sample	All research samples were synthesized and fabricated by the authors of the manuscript in the laboratory. Various control experiments were conducted to test the validity of our hypothesis or to determine the specific cause of an observed effect.
Sampling strategy	In this particular field, reporting data in triplicate is considered a standard practice to enhance the robustness and credibility of the results.
Data collection	All experimental data were collected by the authors of the manuscript using specific apparatuses described in "Experiment Section" .
Timing and spatial scale	The data reported were collected between Jan 1, 2020 - Oct 31, 2022. All the experiment were performed in a laboratory under simulated sunlight with a controlled environment except for the integrated experiments that were performed under natural sunlight on Aug 6, 2022
Data exclusions	No data were excluded from the analysis.
Reproducibility	Reported values are based on triplicates except for the integrated and large-scale experiments, where the values from the duplicates and a single experiment were reported, respectively. The errors correspond to the standard deviation of data points from individual samples. All attempts to repeat the experiment were successful.
Randomization	Randomization is not commonly used in solar fuels research because it typically involves complex design and testing that are difficult to randomly control and manipulate. In addition, our work required specific conditions and carefully designed systems to achieve high system efficiency. Therefore, systematic and controlled experimentation were used over randomization in this work.
Blinding	Our work involves the design, development, extensive testing and characterization of materials and systems, which is not typically subject to bias or confounding factors that would require blinding. Instead, various control experiments were conducted to isolate and evaluate the impact of a each variable.

Did the study involve field work? ☐ Yes ☒ No

Reporting for specific materials, systems and methods

We require information from authors about some types of materials, experimental systems and methods used in many studies. Here, indicate whether each material, system or method listed is relevant to your study. If you are not sure if a list item applies to your research, read the appropriate section before selecting a response.

Materials & experimental systems

n/a	Involved in the study
☒	☐ Antibodies
☒	☐ Eukaryotic cell lines
☒	☐ Palaeontology and archaeology
☒	☐ Animals and other organisms
☒	☐ Clinical data
☒	☐ Dual use research of concern

Methods

n/a	Involved in the study
☒	☐ ChIP-seq
☒	☐ Flow cytometry
☒	☐ MRI-based neuroimaging